

ON THE PENETRATION OF MERIDIONAL CIRCULATION BELOW THE SOLAR CONVECTION ZONE

P. GARAUD & N. H. BRUMMELL

Department of Applied Mathematics and Statistics, Baskin School of Engineering, University of California Santa Cruz, 1156

High Street, CA 95064 Santa Cruz, USA

Draft version August 30, 2021

ABSTRACT

Meridional flows with velocities of a few meters per second are observed in the uppermost regions of the solar convection zone. The amplitude and pattern of the flows deeper in the solar interior, in particular near the top of the radiative region, are of crucial importance to a wide range of solar magnetohydrodynamical processes. In this paper, we provide a systematic study of the penetration of large-scale meridional flows from the convection zone into the radiative zone. In particular, we study the effects of the assumed boundary conditions applied at the convective-radiative interface on the deeper flows. Using simplified analytical models in conjunction with more complete numerical methods, we show that penetration of the convectively-driven meridional flows into the deeper interior is not necessarily limited to a shallow Ekman depth but can penetrate much deeper, depending on how the convective-radiative interface flows are modeled.

Subject headings: hydrodynamics — method:numerical — method:analytical — Sun:interior

1. INTRODUCTION

Meridional flows in the solar interior have recently become the focus of observational and theoretical attention. Poleward sub-surface flows with amplitudes of the order of a few tens of meters per second have been detected with reliable accuracy down to about $0.85r_{\odot}$ (Giles *et al.* 1997). A globally equatorward return flow must exist deeper in the interior to guarantee mass conservation, but its amplitude and structure can only be conjectured currently. This paper addresses the question of how deeply these meridional flows penetrate into the radiative zone. An understanding of these return meridional flows is of fundamental importance since their nature plays a crucial role in many current theories for the internal magneto-hydrodynamics of the Sun.

Firstly, meridional circulations have been argued to play a central role in the operation of the global solar dynamo (see the review by Charbonneau, 2005). In these models, the predicted spatio-temporal behavior of the solar cycle depends sensitively on the assumed circulation pattern and speed. The chosen position for the return flow coupled with mass conservation sets the velocity of the equatorward flow near the base of the convection zone and therefore controls the activity cycle period. Similarly, the depth of penetration of the meridional flows into the radiative region determines where the toroidal magnetic field is generated, and therefore also influences the cycle period and the field amplitudes.

Secondly, meridional flows advect angular momentum, and therefore play a key role in the global dynamical balance of the solar interior. For example, helioseismology has revealed the existence of a strong radial shear layer, now known as the solar tachocline (Brown *et al.* 1989; Spiegel & Zahn, 1992; Hughes, Rosner & Weiss, 2007), located precisely at the interface between the radiative and convective regions. Quantitative models of the tachocline have revealed a sensitive dependence of the interior angular velocity profile on the derived or assumed interfacial flows (Spiegel & Zahn, 1992; Gough & McIntyre, 1998; Rempel, 2005; Garaud, 2007).

Finally, meridional flows also transport various chemical species within the solar interior, with directly observable con-

sequences. Near the base of the convection zone, mixing by large-scale flows can prevent the gravitational settling of helium with respect to hydrogen, leaving a noticeable signature in the helioseismic sound-speed data (Elliott & Gough, 1999). Additional mixing below the convection zone in the main-sequence phase is also required by the observed surface abundances of light elements such as lithium and beryllium, with plausibly the same origin.

Flows with amplitudes on the order of tens of meters per second are required to balance angular momentum transport by the turbulent stresses throughout the convection zone (Miesch *et al.* 2000). Since there exist no physical barrier between the convective and radiative regions, these convectively driven flows may continue their downward progress somewhat beyond the driving region into the radiative zone, thereby “penetrating” or “overshooting” into the interior while retaining potentially significant velocities. How far flows extend beyond their driving region is an essential question.

The problem has recently been addressed by Gilman & Miesch (2004) (GM04 hereafter) and by McIntyre (2007). Using a steady-state formalism, GM04 discuss the depth of penetration of an existing *latitudinal* flow into the radiative interior. They argue that the source flow amplitude is rapidly damped in the radiative interior within a shallow Ekman depth. This depth ranges from a fraction of a kilometer, using microscopic values of the viscosity, to a few tens of kilometers, using a turbulent value of the viscosity. Gilman and Miesch reach a strong conclusion, namely that “*the physics of the solar tachocline and neighboring regions does not allow penetration of meridional circulation originating in the solar convection zone below the overshoot layer*”. This could have dramatic consequences for the magneto-hydrodynamics of the solar radiative zone.

However, steady-state solutions are sensitively dependent on boundary conditions. GM04 solve the problem for the radiative interior dynamics where the forcing is by purely latitudinal flows at the upper convective-radiative interface. They do not consider interfacial forcing from flows generated by the differential rotation nor by direct radial pumping into the radiative zone (only radial flows generated for mass conservation in response to their latitudinal forcing). It is reasonable to address

the question as to whether their strong conclusion remains applicable under more general circumstances.

In this paper, we therefore extend the work of GM04 to allow for greater generality in the source forcing flow, allowing the possibility of azimuthal and radial flows in addition to the latitudinal flows. We systematically examine the consequences of using these various sets of boundary conditions to mimic the convective-radiative interface. We find that the meridional flows can penetrate to significantly different depths, depending upon the choice of boundary conditions. The GM04 solution can be recovered in special cases, but is typically overpowered by other solutions when alternative assumptions are made about the nature of the flows driven within the convection zone.

In what follows, we adopt a three-step approach to study the penetration of meridional flows into the solar radiative zone. Given the added difficulties inherent to spherical coordinate systems, we first examine the problem in Cartesian geometry. In §2, we study analytically the complete set of steady, linear, pseudo-axisymmetric Boussinesq equations and explore a wide range of boundary conditions that may possibly mimic the effects of the convection zone on the radiative zone. We systematically discuss the solutions obtained, which are linear combinations of two fundamental modes of behavior. One of these modes is a solution which varies rapidly on a typical shallow Ekman scale as found by GM04, the other one is a more slowly varying solution which can span the entire interior. In order to gain better insight into the physics of the system and in particular the new solutions, in §3 we consider a simplified Cartesian Boussinesq model in which the solutions related to the Ekman layers are artificially suppressed by neglecting the viscous terms in the radial and latitudinal components of the momentum equation. Finally, in §4, we relax the Cartesian constraint and present numerical results for all of the various boundary conditions in a steady, linear, anelastic, spherical but axisymmetric simulation of the solar radiative zone. We compare these numerical results in spherical geometry with the analytical predictions from the Cartesian models, both in terms of the scale of variation of the solutions, and in terms of their predicted flow velocities. While the spherical geometry as well as the non-uniform background state necessarily add to the complexity of the problem, we find that the analytical scalings extracted from the Cartesian geometry models agree very well with the full numerical solutions. When more complex boundary conditions are taken into account, limits on the penetration of meridional flows into the radiative zone are much less stringent than previously claimed. The exact flow velocities and depth of penetration achieved, however, depend sensitively on the actual boundary conditions selected. These results and conclusions are discussed in detail in §5.

2. A CARTESIAN MODEL

In all that follows we consider a stably stratified radiative zone located beneath a turbulent convection zone, a typical situation encountered in all solar-type stars. Within the convection zone, we assume that turbulent stresses drive large-scale flows in the azimuthal direction (i.e. a large-scale differential rotation) as well as in the meridional direction. The amplitude and spatial variation of the flows just above the convective-radiative interface is assumed to be known. We then pose and solve the following question: *What is the resulting flow pattern and velocities in the underlying radiative zone?*

2.1. Model setup

The spherical geometry of the solar radiative zone as well as the non-uniform background state (in terms of temperature and density, viscosity and thermal conductivity for instance) both preclude any attempt at solving the problem analytically. We postpone to §4 the presentation and discussion of the complete numerical solution of the problem, and first consider a much simplified “radiative zone” with rectangular geometry in Cartesian coordinates (x, y, z) , and a uniform background temperature gradient, viscosity and thermal conductivity. In this coordinate system, the x -direction can be thought of as the azimuthal direction with $x \in [0, 2\pi R]$, the y -direction is aligned with the latitudinal direction and is limited to $y \in [0, \pi R]$ and finally the z -direction is the radial direction with $z \leq R$. The poles are represented by $y = 0$ and $y = \pi R$ while the equator is at $y = \pi R/2$. The dimensional constant R represents the base of the convection zone, and $z = 0$ the interior of the Sun. The system rotates with angular velocity $\Omega = (0, 0, \Omega)$, and gravity is assumed to be aligned with the rotation axis.

2.2. Model equations and general solution

The equations governing dynamical and thermal perturbations to a stably stratified background assumed at rest are the mass, momentum and thermal energy conservation equations. Using the Boussinesq approximation and assuming “axial” symmetry (i.e. $\partial/\partial x = 0$), we first linearize these equations in the thermal perturbations and flow velocities, then project them onto the Cartesian coordinate system as

$$\begin{aligned} \frac{\partial v}{\partial y} + \frac{\partial w}{\partial z} &= 0, \\ -2\Omega v &= \nu \left(\frac{\partial^2 u}{\partial y^2} + \frac{\partial^2 u}{\partial z^2} \right), \\ 2\Omega u &= -\frac{\partial p}{\partial y} + \nu \left(\frac{\partial^2 v}{\partial y^2} + \frac{\partial^2 v}{\partial z^2} \right), \\ 0 &= -\frac{\partial p}{\partial z} + g\alpha\theta, \\ \beta w &= \kappa \left(\frac{\partial^2 \theta}{\partial y^2} + \frac{\partial^2 \theta}{\partial z^2} \right), \end{aligned} \quad (1)$$

where $\mathbf{u} = (u, v, w)$ is the flow velocity, θ is the temperature perturbation, ν and κ are the viscosity and thermal diffusivity, $\alpha = 1/\bar{T}$ where \bar{T} is the background temperature and finally, $g\alpha\beta = N^2$ is the background buoyancy frequency. Note that the viscous diffusion term in the radial component of the momentum equation has been neglected in accordance with hydrostatic equilibrium; this does not affect in any way the conclusions of this paper.

While GM04 and McIntyre (2007) neglected the $\partial^2/\partial y^2$ terms in the viscous terms, we consider here for completeness the full Laplacian. The additional terms are found to be necessary in the light of the fact that some of the boundary layers in the system are large compared with the vertical size of the domain. Neglecting these terms is not physically justified, and mathematically transforms any slowly varying, standard exponential solutions into the rather unphysical secular linear solutions described by McIntyre (2007) (and neglected by GM04).

The hydrostatic equilibrium equation can be combined with the latitudinal component of the momentum equation to yield a generalized thermal-wind equation,

$$2\Omega \frac{\partial u}{\partial z} + \alpha g \frac{\partial \theta}{\partial y} = \nu \frac{\partial}{\partial z} \left(\frac{\partial^2 v}{\partial y^2} + \frac{\partial^2 v}{\partial z^2} \right). \quad (2)$$

Seeking solutions with latitudinal dependence as $\sin(2ny/R)$ or $\cos(2ny/R)$, and exponential vertical dependence as $\exp(kz)$, we obtain the characteristic equation

$$\left(k^2 - \frac{4n^2}{R^2}\right) \left[k^2 \left(k^2 - \frac{4n^2}{R^2}\right)^2 + \frac{k^2}{d_E^4} - \frac{4n^2}{R^2 d_{BD}^4} \right] = 0, \quad (3)$$

where we have introduced two standard characteristic length-scales

$$d_E = \left(\frac{\nu}{2\Omega}\right)^{1/2} \text{ and } d_{BD} = \left(\frac{\nu\kappa}{N^2}\right)^{1/4}, \quad (4)$$

the first one being the standard Ekman depth and the second representing a buoyancy-diffusion layer (GM04, Barcildon & Pedlosky 1967).

It is possible to show (with some algebra) that in the limit where

$$\frac{R^4 d_{BD}^8}{16n^4 d_E^{12}} \gg 1, \quad (5)$$

(which is always true below the base of the convection zone) then the eight solutions to equation (3) ($\pm k_1, \pm k_2, \pm k_3$ and $\pm k_4$) can be approximated by

$$\begin{aligned} k_1 &= \frac{2n}{R}, \\ k_2 &\simeq \frac{d_E^2}{d_{BD}^2} \frac{2n}{R}, \\ k_{3,4} &\simeq \frac{\sqrt{2}}{2} (1 \pm i) d_E^{-1}, \end{aligned} \quad (6)$$

thus yielding four slowly varying exponential solutions (related to k_1 and k_2) in addition to four rapidly varying, oscillatory and exponential solutions related to k_3 and k_4 which describe the Ekman layers of the system. The Ekman solutions were found and described by GM04. On the other hand, the $\pm k_1$ and $\pm k_2$ solutions differ from the (two) real solutions found by GM04, a discrepancy which can easily be traced back to the omitted $\partial^2/\partial y^2$ in their viscous diffusion terms.

It is interesting to note that

$$k_2 = \sqrt{PrBu} \frac{n}{D} = \sqrt{PrBu} \frac{R}{2D} k_1, \quad (7)$$

where D is the local density scaleheight, $Pr = \nu/\kappa$ is the Prandtl number and where the Burger number Bu is defined as

$$Bu = \left(\frac{ND}{R\Omega}\right)^2. \quad (8)$$

The Burger number in the solar radiative zone is estimated to be about $Bu \simeq 2.5 \times 10^3$ using $\Omega = 2.7 \times 10^{-6} \text{s}^{-1}$, $N = 8 \times 10^{-4} \text{s}^{-1}$, $R = 5 \times 10^{10} \text{cm}$ and $D = 0.17R = 8.6 \times 10^9 \text{cm}$ (see Gough, 2007). In laminar regions of the solar radiative zone, the microscopic Prandtl number is of order $Pr = 2 \times 10^{-6}$, so that

$$k_2^{-1} \simeq 5k_1^{-1}, \quad (9)$$

which is clearly of the order of R itself for large-scale forcing (small n).

2.3. General solutions

Consider for instance the solution of (1) corresponding to $\cos(2ny/R)$ and $\sin(2ny/R)$ variations in the azimuthal velocity:

$$\begin{aligned} u(x, y, z) &= (a_1 e^{k_1 z} + a_2 e^{-k_1 z} + a_3 e^{k_2 z} + a_4 e^{-k_2 z}) \\ &+ a_5 e^{k_3 z} + a_6 e^{-k_3 z} + a_7 e^{k_4 z} + a_8 e^{-k_4 z}) \cos\left(\frac{2ny}{R}\right) \\ &+ (b_1 e^{k_1 z} + b_2 e^{-k_1 z} + b_3 e^{k_2 z} + b_4 e^{-k_2 z} \\ &+ b_5 e^{k_3 z} + b_6 e^{-k_3 z} + b_7 e^{k_4 z} + b_8 e^{-k_4 z}) \sin\left(\frac{2ny}{R}\right). \end{aligned} \quad (10)$$

This corresponds to

$$\begin{aligned} v(x, y, z) &= d_E^2 \left[(k_1^2 - k_2^2) (a_3 e^{k_2 z} + a_4 e^{-k_2 z}) \right. \\ &+ (k_1^2 - k_3^2) (a_5 e^{k_3 z} + a_6 e^{-k_3 z}) \\ &+ (k_1^2 - k_4^2) (a_7 e^{k_4 z} + a_8 e^{-k_4 z}) \left. \right] \cos\left(\frac{2ny}{R}\right) \\ &+ d_E^2 \left[(k_1^2 - k_2^2) (b_3 e^{k_2 z} + b_4 e^{-k_2 z}) \right. \\ &+ (k_1^2 - k_3^2) (b_5 e^{k_3 z} + b_6 e^{-k_3 z}) \\ &+ (k_1^2 - k_4^2) (b_7 e^{k_4 z} + b_8 e^{-k_4 z}) \left. \right] \sin\left(\frac{2ny}{R}\right), \end{aligned} \quad (11)$$

$$\begin{aligned} w(x, y, z) &= d_E^2 \left[\frac{k_1}{k_2} (k_1^2 - k_2^2) (a_3 e^{k_2 z} - a_4 e^{-k_2 z}) \right. \\ &+ \frac{k_1}{k_3} (k_1^2 - k_3^2) (a_5 e^{k_3 z} - a_6 e^{-k_3 z}) \\ &+ \frac{k_1}{k_4} (k_1^2 - k_4^2) (a_7 e^{k_4 z} - a_8 e^{-k_4 z}) \left. \right] \sin\left(\frac{2ny}{R}\right) \\ &- d_E^2 \left[\frac{k_1}{k_2} (k_1^2 - k_2^2) (b_3 e^{k_2 z} - b_4 e^{-k_2 z}) \right. \\ &+ \frac{k_1}{k_3} (k_1^2 - k_3^2) (b_5 e^{k_3 z} - b_6 e^{-k_3 z}) \\ &+ \frac{k_1}{k_4} (k_1^2 - k_4^2) (b_7 e^{k_4 z} - b_8 e^{-k_4 z}) \left. \right] \cos\left(\frac{2ny}{R}\right), \end{aligned} \quad (12)$$

and finally

$$\begin{aligned} \theta(x, y, z) &= -\frac{2\Omega}{g\alpha} \left[(a_1 e^{k_1 z} - a_2 e^{-k_1 z}) + \frac{k_2}{k_1} (a_3 e^{k_2 z} - a_4 e^{-k_2 z}) \right. \\ &+ \frac{k_2^2}{k_1 k_3} (a_5 e^{k_3 z} - a_6 e^{-k_3 z}) + \frac{k_2^2}{k_1 k_4} (a_7 e^{k_4 z} - a_8 e^{-k_4 z}) \left. \right] \\ &\cdot \sin\left(\frac{2ny}{R}\right) \\ &+ \frac{2\Omega}{g\alpha} \left[(b_1 e^{k_1 z} - b_2 e^{-k_1 z}) + \frac{k_2}{k_1} (b_3 e^{k_2 z} - b_4 e^{-k_2 z}) \right. \\ &+ \frac{k_2^2}{k_1 k_3} (b_5 e^{k_3 z} - b_6 e^{-k_3 z}) + \frac{k_2^2}{k_1 k_4} (b_7 e^{k_4 z} - b_8 e^{-k_4 z}) \left. \right] \\ &\cdot \cos\left(\frac{2ny}{R}\right), \end{aligned} \quad (13)$$

where one must bear in mind that k_1 and k_2 depend on the wavenumber n/R of the forcing function.

2.4. Boundary conditions

To find the amplitude of each exponential term, one must apply the boundary conditions to the general solutions. A quick look at the system shows that eight boundary conditions are required, which arise from conditions on u , v , w and θ at both the top and bottom of the domain.

We choose boundary conditions at $z = R$ to represent the action of the convection zone on the underlying stably stratified and laminar radiative region. We require the continuity of the radiative interior solution with the complete vector of velocities at the base of the convection zone, so that

$$\mathbf{u}(x, y, R) = \mathbf{u}_{cz}(y) = (u_{cz}(y), v_{cz}(y), w_{cz}(y)) \quad (14)$$

(where the meridional and azimuthal flows in the convection zone are assumed to be axisymmetric). A simple reasonable prescription for the flow velocities at the interface might be, for instance,

$$\begin{aligned} u_{cz}(y) &= -U_0 \cos\left(\frac{2y}{R}\right), \\ v_{cz}(y) &= V_0 \sin\left(\frac{2y}{R}\right), \\ w_{cz}(y) &= -W_0 \cos\left(\frac{2y}{R}\right). \end{aligned} \quad (15)$$

The azimuthal forcing term $u_{cz}(y)$ represents a solar-like differential rotation (with slower-than-average rotation near the poles and faster-than-average rotation near the equator if $U_0 > 0$). The latitudinal and radial forcing terms $v_{cz}(y)$ and $w_{cz}(y)$ represent a single-cell flow in each hemisphere with independent vertical and latitudinal flow velocities. When $V_0 > 0$ the flow is equatorward at the boundary, while $W_0 > 0$ guarantees inflow in the high latitudes and outflow in the low latitudes. Note that since the problem studied is linear, and since any of the three velocity components of $(u_{cz}(y), v_{cz}(y), w_{cz}(y))$ can be written as a Fourier series in $\cos(2ny/R)$ and $\sin(2ny/R)$, it is possible to find the general solution of (1) for any set of imposed velocities. The profiles chosen here contain only one Fourier component for simplicity.

Near the bottom boundary, we would in principle like to choose boundary conditions that have as little effect on the solution as possible. In the real Sun they would instead be replaced by regularity conditions at the origin. However, fitting eight boundary conditions to the general solutions yields an 8×8 linear system which is difficult to study analytically (even with the help of Maple or equivalent software). Thus in this section we restrict our study to the case where the bottom boundary is located at $z \rightarrow -\infty$. This immediately implies that all of the even $\{a_i\}$ and $\{b_i\}$ coefficients must be null. In §3 we revisit this simplification, and suggest an easy way of deducing the solutions in a geometry where the bottom boundary is at $z = 0$ from those in a semi-infinite domain. In §4 we verify our hypothesis against numerical results.

In what follows (§2.5 and §2.6) we describe two possibilities for the thermal boundary conditions at the convective-radiative interface.

2.5. Thermal boundary conditions of type 1: “perfectly” conducting convection zone

The local heat flux through the boundary associated with the perturbations is the sum of the conducted heat flux $-k\partial\theta/\partial z$ and the advected heat flux $\bar{\rho}\bar{h}w$, where $\bar{\rho}$ is the background density, \bar{h} is the background enthalpy, and $k = \bar{\rho}c_p\kappa$ is the thermal conductivity (here c_p is the specific heat at constant pressure).

In a steady-state this local heat flux must be equal to zero, so that when the convection zone is perfectly conducting ($k \rightarrow \infty$) the thermal boundary condition reduces to $\partial\theta/\partial z = 0$.

Using this final boundary condition together with the ones described in §2.4 we find that the remaining odd coefficients $\{a_i\}_{i=1,3,5,7}$ satisfy the linear system $MA = C$ with

$$M = \begin{pmatrix} 1 & 1 & 1 & 1 \\ 0 & k_1^2 - k_2^2 & k_1^2 - k_3^2 & k_1^2 - k_4^2 \\ 0 & \frac{k_1^2 - k_2^2}{k_2} & \frac{k_1^2 - k_3^2}{k_3} & \frac{k_1^2 - k_4^2}{k_4} \\ k_1^2 & k_2^2 & k_2^2 & k_2^2 \end{pmatrix} \quad (16)$$

and

$$A = \begin{pmatrix} a_1 e^{k_1 R} \\ a_3 e^{k_2 R} \\ a_5 e^{k_3 R} \\ a_7 e^{k_4 R} \end{pmatrix} \text{ and } C = \begin{pmatrix} -U_0 \\ 0 \\ 0 \\ 0 \end{pmatrix}. \quad (17)$$

Similarly, the coefficients $\{b_i\}_{i=1,3,5,7}$ satisfy the system $MB = D$ with

$$B = \begin{pmatrix} b_1 e^{k_1 R} \\ b_3 e^{k_2 R} \\ b_5 e^{k_3 R} \\ b_7 e^{k_4 R} \end{pmatrix} \text{ and } D = \begin{pmatrix} 0 \\ V_0 d_E^{-2} \\ W_0 d_E^{-2} k_1^{-1} \\ 0 \end{pmatrix}. \quad (18)$$

In the limit where $k_2 \ll k_1 \ll |k_3|, |k_4|$ the solutions can be simplified to yield

$$\begin{aligned} a_1 &\simeq U_0 \frac{k_2^2}{k_1^2} e^{-k_1 R}, \\ a_3 &\simeq -U_0 e^{-k_2 R}, \\ a_5 &\simeq U_0 \frac{k_1^2}{k_2} \frac{k_4}{k_3(k_3 - k_4)} e^{-k_3 R}, \\ a_7 &\simeq U_0 \frac{k_1^2}{k_2} \frac{k_3}{k_4(k_4 - k_3)} e^{-k_4 R}, \end{aligned} \quad (19)$$

and

$$\begin{aligned} b_1 &\simeq 0, \\ b_3 &\simeq \left[-\frac{V_0}{d_E^2} \frac{1}{k_3 k_4} + \frac{W_0}{d_E^2} \frac{(k_3 + k_4)}{k_1 k_3 k_4} \right] e^{-k_2 R}, \\ b_5 &\simeq \left[-\frac{V_0}{d_E^2} \frac{1}{k_3(k_3 - k_4)} + \frac{W_0}{d_E^2 k_1} \frac{k_4}{k_3(k_3 - k_4)} \right] e^{-k_3 R}, \\ b_7 &\simeq \left[-\frac{V_0}{d_E^2} \frac{1}{k_4(k_4 - k_3)} + \frac{W_0}{d_E^2 k_1} \frac{k_3}{k_4(k_4 - k_3)} \right] e^{-k_4 R}. \end{aligned} \quad (20)$$

We can now finally evaluate, for instance, the latitudinal flow velocity within this rectangular radiative zone:

$$\begin{aligned} v(x, y, z) &\simeq \left[-d_E^2 k_1^2 U_0 e^{k_2(z-R)} - d_E^2 k_1^2 \frac{U_0}{k_2} \frac{k_4 k_3}{k_3 - k_4} e^{k_3(z-R)} \right] \cos\left(\frac{2y}{R}\right) \\ &\quad - d_E^2 k_1^2 \frac{U_0}{k_2} \frac{k_3 k_4}{k_4 - k_3} e^{k_4(z-R)} \cos\left(\frac{2y}{R}\right) \\ &\quad + \left[\left(-V_0 \frac{k_1^2}{k_3 k_4} + W_0 \frac{k_1(k_3 + k_4)}{k_3 k_4} \right) e^{k_2(z-R)} \right. \\ &\quad + \left(V_0 \frac{k_3}{k_3 - k_4} - \frac{W_0}{k_1} \frac{k_4 k_3}{k_3 - k_4} \right) e^{k_3(z-R)} \\ &\quad \left. + \left(V_0 \frac{k_4}{k_4 - k_3} - \frac{W_0}{k_1} \frac{k_3 k_4}{k_4 - k_3} \right) e^{k_4(z-R)} \right] \sin\left(\frac{2y}{R}\right). \end{aligned} \quad (21)$$

As expected from the linearity of the governing system equations (1), the meridional flow velocity in the radiative interior is simply the sum of the three contributions arising from azimuthal forcing only (with terms proportional to U_0), latitudinal forcing only (with terms proportional to V_0) and radial forcing only (with terms proportional to W_0). In addition, each of these three contributions is the sum of three terms, one with exponential dependence in $e^{k_2(z-R)}$ which corresponds to a very slowly varying function of depth, and two complex conjugate terms with exponential dependence in $e^{k_3(z-R)}$ and $e^{k_4(z-R)}$ associated with the very rapidly decaying and oscillating Ekman solutions.

We now compare the relative amplitudes of all of these terms as a function of the parameters of the system. The amplitude

of the rapidly decaying component of the solution arising from azimuthal forcing only is

$$d_E^2 k_1^2 \frac{U_0}{k_2} \left| \frac{k_3 k_4}{k_3 - k_4} \right| \simeq \sqrt{\frac{8E_\nu}{PrBu}} \frac{D}{R} U_0 \quad (22)$$

using the values of k_i derived in equations (6) and (7), and where

$$E_\nu = \frac{\nu}{R^2 \Omega} = \frac{2d_E^2}{R^2} \quad (23)$$

is the Ekman number. Similarly, the slowly decaying component of the solution arising from azimuthal forcing only has an amplitude

$$d_E^2 k_1^2 U_0 \simeq 2E_\nu U_0 \quad (24)$$

Given that $E_\nu \simeq 10^{-16}$ near the base of the convection zone for microscopic values of the viscosity, within an Ekman length of the boundary both components of the solution are negligible.

Similarly with the other forcing contributions, we conclude that

- latitudinal forcing drives meridional flows with a rapidly decaying component which has an amplitude V_0 (with no dependence on any of the other parameters of the system), while the slowly decaying component has an amplitude proportional to $E_\nu V_0$. Thus, in agreement with the study of GM04, we find that within a few Ekman lengths, both are negligible for microscopic values of the viscosity.
- radial forcing drives meridional flows with a rapidly decaying component which has an amplitude proportional to $W_0/\sqrt{E_\nu}$, while the slowly decaying component has an amplitude proportional to $\sqrt{E_\nu} W_0$. Thus, in this particular case we find that beyond a few Ekman lengths the slow mode retains a non-negligible amplitude of about 10^{-8} times the imposed velocity. Indeed, for imposed meter per second flow velocities, the flows near the top of the radiative zone could then be of the order of $\sqrt{E_\nu} W_0 \simeq 10^{-6}$ centimeters per second, with an overall turnover time of the order of $R/\sqrt{E_\nu} W_0 \simeq 1$ Gyr. While very slow, this can still provide mixing in the tachocline on the stellar evolution and/or gravitational settling timescale.

2.6. Thermal boundary conditions of type 2: no net perturbed heat flux through the boundary

Dropping the assumption that the convection zone is a perfectly conducting fluid, we require instead that $\overline{hw} = c_p \kappa \partial \theta / \partial z$, which is equivalent to $\overline{T}w = \kappa \partial \theta / \partial z$.

We can rewrite this new thermal boundary condition into the linear systems $MA = C$ and $MB = E$ where M , A , B and C have already been defined, and

$$E = \begin{pmatrix} 0 \\ V_0 d_E^{-2} \\ W_0 d_E^{-2} k_1^{-1} \\ -W_0 k_2^2 H_\Theta / d_E^2 k_1 \end{pmatrix}, \quad (25)$$

where H_Θ is the potential temperature scaleheight

$$H_\Theta = \frac{\overline{T}}{\beta} = \frac{g}{N^2}. \quad (26)$$

Thus the $\{a_i\}$ coefficients are the same as in the previous section, while in the limit where $k_2 \ll k_1 \ll |k_3|, |k_4|$

$$\begin{aligned} b_1 &\simeq -\frac{H_\Theta k_2^2}{d_E^2 k_1^3} W_0 e^{-k_1 R}, \\ b_3 &\simeq \left(-\frac{V_0}{k_3 k_4} + \frac{H_\Theta k_2^2}{k_1^3} W_0 \right) \frac{e^{-k_2 R}}{d_E^2}, \\ b_5 &\simeq -\left[V_0 + W_0 \frac{k_4}{k_1} (H_\Theta k_2 - 1) \right] \frac{e^{-k_3 R}}{k_3 (k_3 - k_4) d_E^2}, \\ b_7 &\simeq -\left[V_0 + W_0 \frac{k_3}{k_1} (H_\Theta k_2 - 1) \right] \frac{e^{-k_4 R}}{k_4 (k_4 - k_3) d_E^2}, \end{aligned} \quad (27)$$

so that

$$\begin{aligned} v(x, y, z) &\simeq \left[-d_E^2 k_1^2 U_0 e^{k_2(z-R)} - d_E^2 k_1^2 \frac{U_0}{k_2} \frac{k_4 k_3}{k_3 - k_4} e^{k_3(z-R)} \right. \\ &\quad \left. - d_E^2 k_1^2 \frac{U_0}{k_2} \frac{k_3 k_4}{k_4 - k_3} e^{k_4(z-R)} \right] \cos\left(\frac{2y}{R}\right) \\ &\quad + \left[\left(-\frac{V_0 k_1^2}{k_3 k_4} + \frac{H_\Theta k_2^2}{k_1} W_0 \right) e^{k_2(z-R)} \right. \\ &\quad \left. + \left(V_0 + W_0 \frac{k_4}{k_1} (H_\Theta k_2 - 1) \right) \frac{k_3 e^{k_3(z-R)}}{k_3 - k_4} \right. \\ &\quad \left. + \left(V_0 + W_0 \frac{k_3}{k_1} (H_\Theta k_2 - 1) \right) \frac{k_4 e^{k_4(z-R)}}{k_4 - k_3} \right] \sin\left(\frac{2y}{R}\right). \end{aligned} \quad (28)$$

For this new set of boundary conditions, azimuthal forcing and latitudinal forcing yield the same solutions as in the previous section, while radial forcing drives meridional flows with a rapidly decaying component which has an amplitude proportional to $W_0(H_\Theta k_2 - 1)/\sqrt{E_\nu}$, while the slowly decaying component has an amplitude proportional to $(H_\Theta/R)(R/D)^2 PrBu W_0$. Note how in this case the slowly decaying component of the flow has an amplitude which is independent of the background viscosity ν .

2.7. Discussion of the solutions

Using this Cartesian geometry model, we have shown that there exist solutions for meridional flows in the radiative interior with significant amplitude throughout. These flows can only be present if driven by direct pumping into and out of the radiative zone, that is, when $w_{cz}(y)$ has a significant amplitude on the boundary. Our study also shows that the actual amplitude of the flows within the radiative zone depends sensitively on the thermal boundary conditions used. While it is not clear which set of boundary conditions actually accurately represents the true convective-radiative interface, it is not implausible that they may lie somewhere in between the two extreme cases studied. Thus it is also not implausible that there may be significant penetration of the convective zone flows into the radiative zone, with typical turnover times shorter than $R/\sqrt{E_\nu} W_0$.

Our results extend the work of GM04, and naturally recover their solutions in the limit where only latitudinal forcing is taken into account. Note that GM04 do not specifically require that w be null on the convective-radiative interface, and argue that any spatially varying latitudinal flow drives radial flows into and out of the boundary to guarantee mass conservation. This is indeed correct, but one must keep in mind that $\partial v / \partial y = -\partial w / \partial z$ only relates latitudinal variations in v to the radial derivative of w . Since the derivative is dominated at the base of the convection zone by rapid variation on the Ekman

scale, the mass conservation equation in fact requires that the radial flows in the GM04 solution have an amplitude of the order of $W_0 = V_0 d_E / R$. It is therefore easy to see why their solution yields negligible velocities for the slowly varying component of the flow penetrating into the radiative zone.

Finally, it is crucial to note that since the momentum and energy equations in this study (and the preceding ones by GM04 and McIntyre, 2007) have been linearized, the predicted amplitudes of the flows are linearly dependent on the imposed flow velocities. In reality, this will only be true in the limit where the typical amplitudes of the nonlinear advection terms ($\mathbf{u} \cdot \nabla \mathbf{u}$ for the momentum equation, and $\mathbf{u} \cdot \nabla \theta$ for the energy equation) are indeed much smaller than the corresponding linear terms ($2\Omega \times \mathbf{u}$ for the momentum equation and βw for the energy equation). The nonlinear terms in the momentum equation for example guarantee that no unphysical counter-rotation is allowed. The linearized equations on the other hand scale arbitrarily with the imposed boundary conditions and do allow counter-rotation for certain input parameters, e.g. if the imposed differential rotation profile $u_{cz}(y)$ is large enough or if the meridional flows are too rapid (see Figure 5 for instance). Similarly, the nonlinear terms in the energy equation guarantee that the actual turnover time of the meridional flows cannot be lower than the local thermal diffusion time (over the depth considered), while the linearized equations allow for any values of the turnover time provided the imposed boundary flow velocities are high enough.

From this linearized model, we can therefore say with reasonable confidence that meridional flows can indeed penetrate into the radiative zone, provided their turnover time (typically estimated as $v(d)/d$ where $d = R - z$ is the depth considered) is longer than the local thermal diffusion time (estimated as d^2/κ).

3. A REDUCED CARTESIAN MODEL

One of the remaining issues that needs to be addressed is that of lower boundary. In the previous section, the high-dimensionality of the solution space made it difficult to consider the more realistic situation of a bottom boundary located at $z = 0$. While the Ekman solutions (associated with k_3 and k_4) decay inward/downward so quickly that the presence or absence of a lower boundary cannot affect them, the slowly varying solutions do span the entire radiative region from $z = R$ down to $z = 0$; the location of the lower boundary is expected to have some influence on their amplitude.

Here, we therefore focus on studying the slowly varying solutions only by considering a system in which the Ekman flows are filtered out. This is another way of reducing the dimensionality of the solution space, and enables us to compare the solutions in a semi-infinite domain to the solutions in a finite domain.

3.1. Reduced model equations

We consider the system

$$\begin{aligned} \frac{\partial v}{\partial y} + \frac{\partial w}{\partial z} &= 0, \\ \frac{\partial p}{\partial z} &= \alpha g \theta, \\ 2\Omega u &= -\frac{\partial p}{\partial y}, \\ -2\Omega v &= \nu \left(\frac{\partial^2 u}{\partial y^2} + \frac{\partial^2 u}{\partial z^2} \right), \\ \beta w &= \kappa \left(\frac{\partial^2 \theta}{\partial y^2} + \frac{\partial^2 \theta}{\partial z^2} \right), \end{aligned} \quad (29)$$

in which the viscous diffusion terms within the latitudinal component of the momentum equation has now been removed. This simplification is consistent with the assumptions of geostrophic equilibrium and, as we now prove, effectively filters out the Ekman flows. The system can be reduced to a single partial differential equation for u , for instance, as

$$\frac{\partial^4 u}{\partial z^4} + \left(1 + \frac{d_E^4}{d_{BD}^4} \right) \frac{\partial^2 u}{\partial z^2 \partial y^2} + \frac{d_E^4}{d_{BD}^4} \frac{\partial^4 u}{\partial y^4} = 0. \quad (30)$$

Seeking exponential solutions in z with periodic behavior in y as before yields the characteristic equation:

$$\left(k^2 - \frac{4n^2}{R^2} \right) \left(k^2 - \frac{4n^2}{R^2} \frac{d_E^4}{d_{BD}^4} \right) = 0, \quad (31)$$

with solutions $\pm K_1$ and $\pm K_2$ with

$$\begin{aligned} K_1 &= \frac{2n}{R} = k_1 \text{ and} \\ K_2 &= \frac{2n}{R} \left(\frac{d_E^2}{d_{BD}^2} \right) = k_2. \end{aligned} \quad (32)$$

Thus we recover only the slowly varying solutions of the previous section.

3.2. General solutions

The flow solution to the above system for fixed latitudinal wavenumber n is

$$\begin{aligned} u(x, y, z) &= (A_1 e^{K_1 z} + A_2 e^{-K_1 z} + A_3 e^{K_2 z} + A_4 e^{-K_2 z}) \cos \left(\frac{2ny}{R} \right) \\ &+ (B_1 e^{K_1 z} + B_2 e^{-K_1 z} + B_3 e^{K_2 z} + B_4 e^{-K_2 z}) \sin \left(\frac{2ny}{R} \right) \end{aligned} \quad (33)$$

which also yields

$$\begin{aligned} v(x, y, z) &= d_E^2 (K_1^2 - K_2^2) (A_3 e^{K_2 z} + A_4 e^{-K_2 z}) \cos \left(\frac{2ny}{R} \right) \\ &+ d_E^2 (K_1^2 - K_2^2) (B_3 e^{K_2 z} + B_4 e^{-K_2 z}) \sin \left(\frac{2ny}{R} \right) \end{aligned} \quad (34)$$

and

$$\begin{aligned} w(x, y, z) &= d_E^2 \frac{K_1}{K_2} (K_1^2 - K_2^2) (A_3 e^{K_2 z} - A_4 e^{-K_2 z}) \sin \left(\frac{2ny}{R} \right) \\ &- d_E^2 \frac{K_1}{K_2} (K_1^2 - K_2^2) (B_3 e^{K_2 z} - B_4 e^{-K_2 z}) \cos \left(\frac{2ny}{R} \right) \end{aligned} \quad (35)$$

3.3. Boundary conditions

The governing equations considered form what is apparently a 6th order system in the z direction, and require, in principle,

6 boundary conditions split between the top and bottom boundaries. Naturally, one would like to impose boundary conditions on u , w and θ (one at the top, one at the bottom for each variable). Note that since the viscous terms have been neglected in the equations for hydrostatic and geostrophic equilibrium respectively, one cannot impose a boundary condition on v : the equations contain no stresses that could transfer the boundary information to the rest of the system. However, we see that combining these equations only yields a 4th order partial differential equation for u . This implies that the 6 selected boundary conditions must somehow be redundant, otherwise there will be no solution to the system. In what follows, we therefore only select boundary conditions for u and w at the top and bottom boundaries. Near the top boundary, we consider as before

$$\begin{aligned} u(x, y, R) &= u_{cz}(y), \\ w(x, y, R) &= w_{cz}(y). \end{aligned} \quad (36)$$

When considering a bottom boundary at $z = 0$, we choose impermeable boundary conditions for w , and stress-free boundary conditions for u so that

$$\begin{aligned} \left. \frac{\partial u}{\partial z} \right|_{(x, y, 0)} &= 0, \\ w(x, y, 0) &= 0. \end{aligned} \quad (37)$$

3.4. Solutions for a semi-infinite domain

When the bottom boundary is near $-\infty$, we find that

$$\begin{aligned} A_1 &= -U_0 e^{-K_1 R}, \\ A_2 &= A_3 = A_4 = 0, \\ B_1 &= -\frac{K_2}{K_1(K_1^2 - K_2^2)} \frac{W_0}{d_E^2} e^{-K_1 R}, \\ B_2 &= B_4 = 0, \\ B_3 &= \frac{K_2}{K_1(K_1^2 - K_2^2)} \frac{W_0}{d_E^2} e^{-K_2 R}, \end{aligned} \quad (38)$$

so that

$$v(x, y, z) = \frac{K_2}{K_1} W_0 e^{K_2(z-R)} \sin(K_1 y), \quad (39)$$

which illustrates again how radial forcing can yield non-zero flow amplitudes penetrating deeply into the radiative zone. It is important to note, however, that the predicted flow amplitude is different from that found in §2. This might be attributed to the fact that when viscous effects are taken into account, a fraction of the flow penetrating into the radiative zone is deflected into the very shallow Ekman layers.

3.5. Solutions for a finite domain

When the bottom boundary is located at $z = 0$, we find that

$$\begin{aligned} A_1 &= A_2 = -\frac{U_0}{2 \cosh(K_1 R)}, \\ A_3 &= A_4 = 0, \\ B_1 &= B_2 = -\frac{K_2}{K_1(K_1^2 - K_2^2)} \frac{W_0}{d_E^2} \frac{\cosh(K_2 R)}{2 \sinh(K_2 R) \cosh(K_1 R)} \\ &\simeq -\frac{W_0}{2 d_E^2 K_1^2} \frac{1}{K_1 R \cosh(K_1 R)}, \\ B_3 &= B_4 = \frac{K_2}{K_1(K_1^2 - K_2^2)} \frac{W_0}{d_E^2} \frac{1}{2 \sinh(K_2 R)} \\ &\simeq \frac{W_0}{2 d_E^2 K_1^2} \frac{1}{K_1 R}, \end{aligned} \quad (40)$$

implying

$$\begin{aligned} v(x, y, z) &= \frac{W_0}{\sinh(K_2 R)} \frac{K_2}{K_1} \cosh(K_2 z) \sin(K_1 y) \\ &\simeq \frac{W_0}{K_1 R} \cosh(K_2 z) \sin(K_1 y). \end{aligned} \quad (41)$$

3.6. Consequences

Comparing the expressions in equations (39) and (41), we find that the slowly varying component of the meridional flow in the case of a finite domain has an amplitude that is $1/K_2 R$ times that of the semi-infinite domain case. The difference between the predicted amplitudes for the two geometrical systems (finite and semi-infinite domains) can easily be understood in the light of the fact that the exponential solutions associated with K_1 and K_2 decay on much longer lengthscales than R .

Extrapolating this result to the full Cartesian problem studied in §2, we therefore predict that the slowly varying components of the meridional flows (associated with the k_1 and k_2 wavenumbers) should in fact have an amplitude that is $1/k_2 R$ times that given in (22) and (29); the Ekman components on the other hand decay so rapidly that their amplitude should not be influenced by the presence of a lower boundary. We now revise our estimates of §2.5 and §2.6 to predict that in the case of type 1 boundary conditions ($\partial\theta/\partial z = 0$ at the upper boundary) then

- azimuthal forcing leads to meridional flows with a rapidly decaying component with an amplitude proportional to $\sqrt{E_\nu/PrBu}U_0$, while the slowly decaying component has an amplitude proportional to $E_\nu U_0/\sqrt{PrBu}$.
- latitudinal forcing leads to meridional flows with a rapidly decaying component with an amplitude proportional to V_0 , while the slowly decaying component has an amplitude proportional to $E_\nu V_0/\sqrt{PrBu}$.
- radial forcing leads to meridional flows with a rapidly decaying component with an amplitude proportional to $W_0/\sqrt{E_\nu}$, while the slowly decaying component has an amplitude proportional to $\sqrt{E_\nu/PrBu}W_0$.

In the case of type 2 boundary conditions (where $\kappa\partial\theta/\partial z = \bar{T}w$ at the upper boundary) the flow velocities predicted in the case of azimuthal and latitudinal forcing are the same, while radial forcing drives flows with a rapidly decaying component with an amplitude proportional to $W_0(H_\Theta k_2 - 1)/\sqrt{E_\nu}$ and a slowly decaying component which has an amplitude proportional to $(H_\Theta/R)\sqrt{PrBu}W_0$.

4. NUMERICAL SOLUTIONS IN A SPHERICAL SHELL

4.1. Model setup

To complete this axisymmetric study and illustrate our analytical results numerically, we perform simulations of flows in the solar radiative zone subject to various boundary conditions. The governing equations for the numerical model are derived by perturbing the spherically symmetric equations of stellar structure, moving to a rotating frame of reference and assuming that the velocity perturbations and thermodynamical perturbations to the background spherically symmetric state are

small enough for linearization to be appropriate. Then

$$\begin{aligned} 2\bar{\rho}\bar{\Omega} \times \mathbf{u} &= -\nabla\tilde{p} - \bar{\rho}\nabla\tilde{\Phi} + f\nabla \cdot \Pi, \\ \nabla \cdot (\bar{\rho}\mathbf{u}) &= 0, \\ \bar{\rho}\bar{T}\mathbf{u} \cdot \nabla\tilde{s} &= f\nabla \cdot (\bar{k}\nabla\tilde{T}), \\ \frac{\tilde{p}}{\bar{p}} &= \frac{\tilde{\rho}}{\bar{\rho}} + \frac{\tilde{T}}{\bar{T}}, \end{aligned} \quad (42)$$

where $\mathbf{u} = (u_r, u_\theta, u_\phi)$ is the velocity field in a frame rotating with angular velocity $\bar{\Omega}$, ρ , T , s and p are the standard thermodynamical variables, $k = \bar{\rho}c_p\kappa$ is the thermal conductivity, Π is the viscous stress tensor (which depends on the viscosity ν) and Φ is the gravitational potential. Quantities denoted with bars are background quantities, taken from the standard solar model of Christensen-Dalsgaard *et al.* (1991), while the temperature, pressure and density perturbations are denoted with tildes.

This system is fully consistent with the Cartesian model equations presented in §2, with the added sophistication of the perfect gas equation of state and the anelastic approximation instead of the simpler Boussinesq approximation. This modification is added so that the model equations are consistent with the level of approximation used, but does not affect the nature of the solutions. The centrifugal force associated with the rotation of the background state $\bar{\Omega} \times \bar{\Omega} \times \mathbf{r}$ has been removed to suppress global Eddington-Sweet circulations, which are known to be of very small amplitude, but would otherwise play an important role in this steady-state calculation (see the work of Garaud, 2002, for comparison). Perturbations in the gravitational potential are neglected in accordance with Cowling's approximation.

Note how both diffusion terms have been multiplied by the same factor f . Since the typical Ekman number in the Sun (just below the base of the convection zone) is of the order of 10^{-16} , a unit value of f would lead to Ekman layers about 10^{-8} times size of the domain; the numerical method used is unable to resolve them. Using values of f of the order of $10^7 - 10^9$ instead inflates the Ekman layers artificially to 10^{-4} times the size of the domain or larger, which can then be fully resolved. As an added bonus, varying f provides an easy way of varying the effective viscosity and thermal conductivity without changing the Prandtl number. As a result, the estimated values of k_1 and k_2 are unchanged from the solar value (since k_2 only depends on the Prandtl number), while k_3 and k_4 are a factor of $f^{1/2}$ smaller. As long as $f \ll 10^{15}$, the hierarchy $k_2 \ll k_1 \ll |k_3|, |k_4|$ is respected.

The numerical method of solution is based on the expansion of the governing equations onto a spherical coordinate system (r, θ, ϕ) , followed by their projection onto Chebishev polynomials $T_n(\cos\theta)$, and finally, solution of the resulting ODE system in r using a Newton-Raphson-Kantorovich algorithm. For more detail, see Garaud (2001). The computational domain is limited to the region of the radiative zone within $r \in [0.02, 0.7]r_\odot$. The solution is found to be reasonably insensitive to the position of the lower boundary for this range of parameters.

In order to study the dependence of the amplitude and depth of penetration of the flows on the Ekman number (i.e. on k_3 and k_4), we perform a series of simulations with f ranging from 10^7 to 10^9 . In order to verify the dependence of the amplitude of the solutions on k_2 , we perform similar calculations with a hypothetical Sun where the thermal conductivity in the system of equations (42) is uniformly multiplied by a factor of four throughout the interior, resulting in a Prandtl number artificially decreased by a factor of four compared with its solar value. In that case, k_2 is two times smaller than in the case of the solar

value of the Prandtl number.

In order to study in detail the effects of the boundary conditions on the solutions, we study separately three cases where forcing is respectively in the azimuthal, latitudinal and radial directions only. In the case of radial forcing, we consider the two boundary conditions studied in §2, namely $\partial\tilde{T}/\partial r$ is null on the boundary, and $\kappa\partial\tilde{T}/\partial r = \bar{T}u_r$.

The details of the expressions for the boundary conditions in each case are given below.

4.2. Boundary conditions.

In all of the simulations performed, the lower boundary conditions at $r = 0.02r_\odot$ are the following:

- impermeable condition on the radial velocity,
- stress-free conditions on the tangential velocities u_θ and u_ϕ ,
- conducting condition on the temperature: we assume that the domain within $0.02r_\odot$ is a conducting solid sphere, so that the temperature perturbations satisfy $\nabla^2\tilde{T} = 0$ within, and are regular at $r = 0$. We solve this equation with the requirement that $\tilde{T} \rightarrow 0$ as $r \rightarrow 0$, and derive a matching condition with the temperature fluctuations at the interface.

Near the upper boundary (at $r = 0.7r_\odot$), we consider the following cases:

- azimuthal forcing only: in this case, we set $u_r = u_\theta = 0$ at the boundary (assuming no-slip conditions). Following the results from helioseismology, we set $u_\phi = 0.7r_\odot \sin\theta\tilde{\Omega}$ with $\tilde{\Omega} = \Omega_{\text{eq}}(1 - a\cos^2\theta - b\cos^4\theta) - \bar{\Omega}$, where $\bar{\Omega} = \Omega_{\text{eq}}(1 - a/5 - 3b/35)$ (Gilman, Morrow & DeLuca, 1989), $a = b = 0.15$ and $\Omega_{\text{eq}} = 2.9 \times 10^{-6}\text{s}^{-1}$. The temperature boundary condition is $\partial\tilde{T}/\partial r = 0$.
- latitudinal forcing only: in this case we set $u_r = u_\phi = 0$ at the boundary, and $u_\theta = V_0 \sin\theta \cos\theta$ with $V_0 = 1$ m/s. Note that $u_\phi = 0$ is guaranteed by setting $a = b = 0$, in which case the background angular velocity is $\bar{\Omega} = \Omega_{\text{eq}} = 2.9 \times 10^{-6}\text{s}^{-1}$. The temperature boundary condition is $\partial\tilde{T}/\partial r = 0$.
- radial forcing only: in this case we set $u_\theta = u_\phi = 0$ at the boundary and $u_r = U_0(1 - 3\cos^2\theta)$ with $U_0 = 1$ cm/s. This expression satisfies the global conservation of mass. In this last case, two temperature boundary conditions are explored as in §2, either $\partial\tilde{T}/\partial r = 0$ (type 1) or $\kappa\partial\tilde{T}/\partial r = \bar{T}u_r$ (type 2).

Note that since the governing equations are linear, the amplitudes of each component of the flow defined by (U_0, V_0, W_0) at the boundary can be chosen arbitrarily. Here, they were selected as what may be plausible flow velocities in the lower regions of the convection zone.

4.3. Results

This section summarizes the numerical results for the various simulations performed.

In order to compare quantitatively the numerical solutions with the Cartesian model predictions we study the variation of the latitudinal component of the meridional flow u_θ , both near and far from the boundary, at a fixed latitude fairly close to the

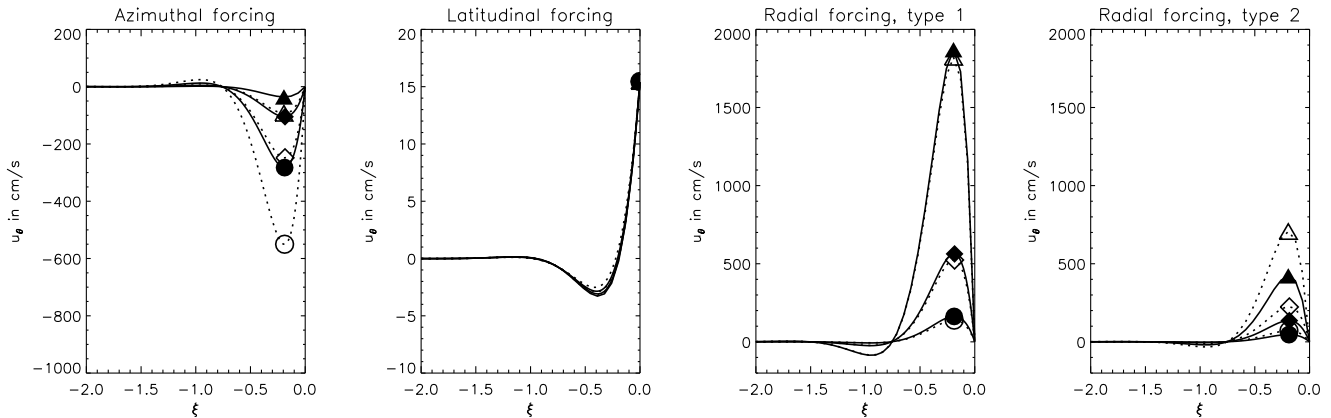


FIG. 1.— Latitudinal velocity at a latitude of 80° as a function of re-scaled depth below the convection zone $\xi = (r - 0.7r_\odot)/d_E$ for the four types of boundary conditions described in §4.2. In each of the four plots, the solid lines (and solid symbols) correspond to simulations with a solar value of the Prandtl number, while the dotted lines (and open symbols) correspond to simulations with a Prandtl number artificially reduced by a factor of four. The symbols identify the value of f used in the simulations: a circle corresponds to $f = 10^9$, a diamond to $f = 10^8$ and a triangle to $f = 10^7$. For comparison, the forcing velocities at the latitude considered are about $u_{cz}(80^\circ) = 5200\text{cm/s}$, $v_{cz}(80^\circ) = 17\text{cm/s}$ and $w_{cz}(80^\circ) = 0.9\text{cm/s}$.

polar regions. We select a high latitude of about 80° since the Cartesian model applies best to systems in which the rotation axis and gravity are nearly aligned.

In Figure 1 we first focus on the region close to the upper boundary in order to single out the Ekman solution. Each plot corresponds to one of the four types of boundary conditions studied, and shows $u_\theta(r)$ at a latitude of about 80° . For clarity, the depth below the convection zone is rescaled with the Ekman depth d_E : thus, in each of the plots $\xi = (r - 0.7r_\odot)/d_E$. The results for the solar value of the Prandtl number are shown in solid lines, and those corresponding to the lower value of the Prandtl number (equivalently, a value of κ that is four times solar) are shown in the dotted lines. In each case, three runs are presented with $f = 10^7$, 10^8 , and 10^9 respectively and can be identified with the symbols. It is immediately obvious from observing all of these plots that there is indeed a component of the solution which decays and oscillates rapidly with depth below the convection zone on an Ekman lengthscale. From the conclusions of §3.6, we expect the amplitude of this rapidly decaying solution to scale as $\sqrt{f/Pr}$ in the case of azimuthal forcing, to be of order of the forcing velocity for any value of f or Pr in the case of the latitudinal forcing, to scale as $1/\sqrt{f}$ for radial forcing with type 1 boundary conditions and finally, to scale as $(H_\Theta k_2 - 1)/\sqrt{f}$ for radial forcing with type 2 boundary conditions. Note that for solar values of the background state and of the Prandtl number, using the standard model of Christensen-Dalsgaard *et al.* (1991), $H_\Theta k_2 \simeq 0.8$; for a Prandtl number that is reduced by a factor of four, then $H_\Theta k_2 \simeq 0.4$.

The comparison between these predicted scalings and the outcome of the numerical simulations is shown in Figure 2. Here, the symbols represent the amplitude of the solution defined as the maximum value achieved by $|u_\theta(r)|$ at the selected latitude, for each of the simulations performed. The lines show the predicted scalings, using as a reference the amplitude of the solution for solar values of the Prandtl number and with $f = 10^7$. Thus, for example, the solid line in the case of azimuthal forcing only is generated by the equation

$$\hat{A}(f, Pr_\odot) = \hat{A}(10^7, Pr_\odot) \left(\frac{f}{10^7} \right)^{1/2} \quad (43)$$

where $\hat{A}(f, Pr_\odot)$ is the predicted amplitude of the other simulations with solar values of the Prandtl number, and $\hat{A}(10^7, Pr_\odot)$

is the numerically calculated reference amplitude of the solution for $f = 10^7$ and solar values of the Prandtl number. The dotted line in the same panel is easily calculated as

$$\hat{A}(f, 0.25Pr_\odot) = 2\hat{A}(10^7, Pr_\odot) \left(\frac{f}{10^7} \right)^{1/2} \quad (44)$$

The solid and dotted lines in the three other panels are constructed in a similar fashion. It is quite clear that the predicted scalings fit the numerical solutions very well, except perhaps in the case of radial forcing with type 2 boundary conditions where the fit is only good to within a factor of order unity. The origin of this discrepancy is not entirely clear, but can be partly traced back to non-ideal effects in the equation of state (which affects the determination of H_Θ) and to geometrical effects (which influence the value of k_2).

In order to compare the scalings of the slowly decaying component of the flow with the numerical results, we now move to Figure 3 and Figure 4 which focus on the behavior of the solution far from the boundary. Figure 3 shows $|u_\theta(r)|$ at a latitude of about 80° throughout the interior on a log-linear scale. The information about the direction of the flow (poleward or equatorward) is lost in this plot, with sign reversals appearing as cusps in the curves pointing towards $-\infty$. Note that it is possible to discern the presence of the Ekman layer close to the outer boundary for the larger values of f .

A quick glance at the solutions in the deep radiative interior reveals the behavior suggested by the Cartesian solutions: different assumptions concerning the boundary conditions yield very different predicted flow velocities. In particular, it can be seen that in the case of radial forcing with type 2 boundary conditions (i.e. $\kappa \partial \tilde{T} / \partial r = \bar{T} u_r$) the flows velocities are more-or-less independent of f , or in other words retain significant amplitudes for any value of the background viscosity.

More quantitatively, from the conclusions of §3.6, we expect the amplitude of the slowly decaying solution to scale as f/\sqrt{Pr} in the case of azimuthal and latitudinal forcing, to scale as $\sqrt{f/Pr}$ for radial forcing with $\partial \tilde{T} / \partial r = 0$ and as $(H_\Theta/R)\sqrt{Pr}$ in the case of radial forcing with the type 2 temperature boundary conditions. The comparison between the predicted scalings and the outcome of the numerical simulations is shown in Figure 4, using the same method as described earlier in the case of the rapidly decaying component of the solution.

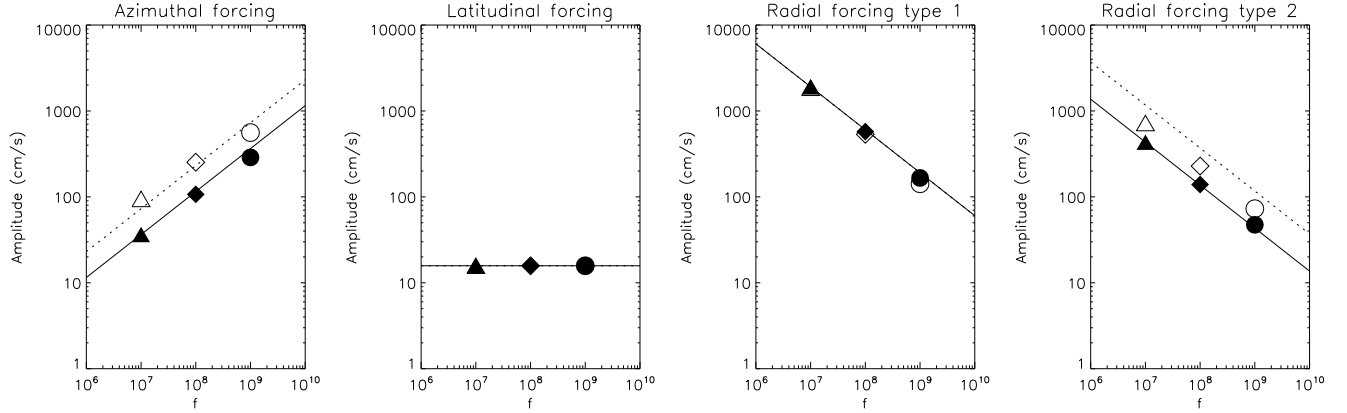


FIG. 2.— Comparison of the scaling of the amplitude of the rapidly decaying solution with the model predictions for the same four types of boundary conditions. For each simulation performed (i.e. for each type of boundary condition, for each value of f and of the Prandtl number considered), the symbols show the maximum value of $|u_\theta(r)|$ found numerically at the latitude considered; note that the same coding is used as in Figure 1. The solid and dotted lines shows the predicted scaling of this amplitude as a function of f for solar values of the Prandtl number and a quarter-times solar value of the Prandtl number respectively. The amplitude of the solution for solar values of the Prandtl number with $f = 10^7$ is used as the reference amplitude.

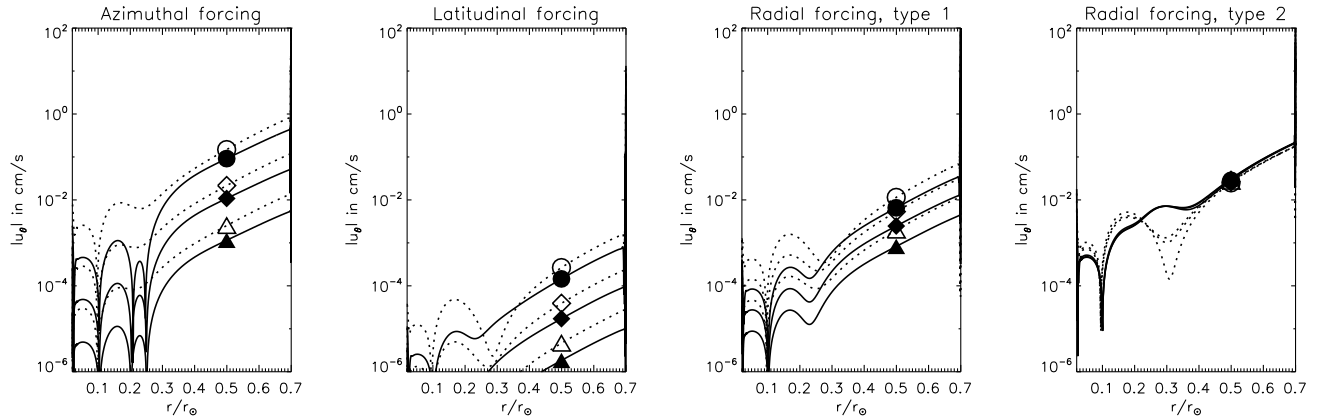


FIG. 3.— Latitudinal velocity of flows below the convection zone as a function of radius for the four types of boundary conditions described in §4.2. The line and symbol coding are the same as in Figure 1.

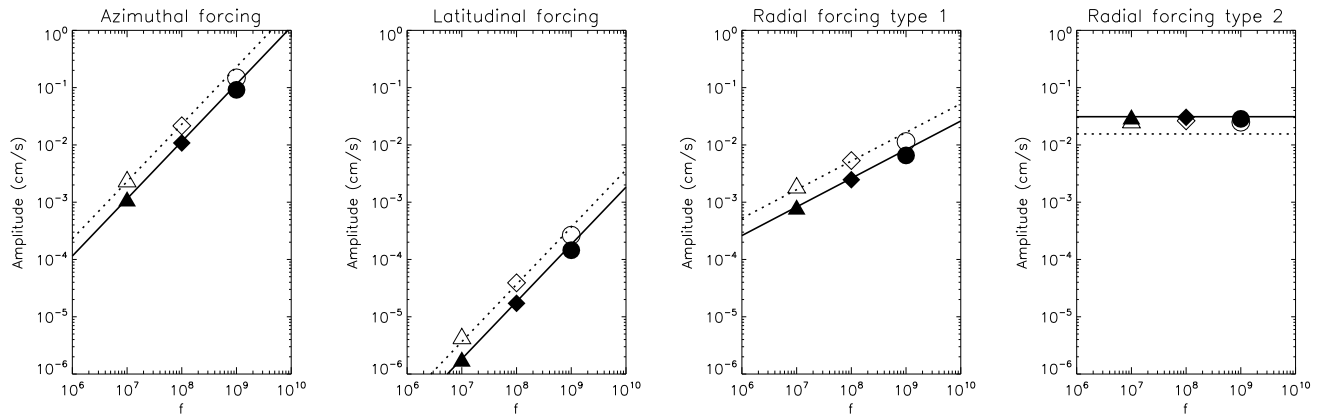


FIG. 4.— Comparison of the scaling of the amplitude of the slowly decaying solution with the model predictions for the same four types of boundary conditions. For each simulation performed (i.e. for each type of boundary condition, for each value of f and of the Prandtl number considered), the symbols show the value of $|u_\theta(0.5r_\odot)|$ found numerically at the latitude considered; again, the same coding is used. The solid and dotted lines shows the predicted scaling of this amplitude as a function of f for solar values of the Prandtl number and a quarter-times solar value of the Prandtl number respectively. The amplitude of the solution for solar values of the Prandtl number with $f = 10^7$ is used as the reference amplitude.

We can see that, as before, the predicted amplitudes agree very well with the numerical solutions, except perhaps in the case of radial forcing with type 2 boundary conditions where a small discrepancy remains.

We therefore conclude that despite the simplified nature of the analytical analysis performed in §2 and §3, the results obtained robustly predict the scalings of the numerical solutions in full spherical geometry.

Finally, in order to provide better insight into the actual solutions, we show in Figure 5 the global structure of the numerical results. In the left-hand-side of Figure 5, we show results for the solar value of the Prandtl number (and therefore solar values of k_2 near the convective-radiative interface), while in the right-hand-side we show results for a quarter-times solar value of the Prandtl number. All the plots were generated for a fixed value of $f = 10^8$ (and therefore 10^8 -times solar values of the viscosity corresponding to 10^{-4} -times solar values of k_3 and k_4). The left quadrants show contour-lines of the stream-function, or in other words, streamlines of the flow while the right quadrants show the angular velocity profile. The four aforementioned boundary conditions are explored: azimuthal forcing only, latitudinal forcing only, radial forcing only with type 1 boundary conditions ($\partial\tilde{T}/\partial r = 0$) and radial forcing only with type 2 boundary conditions ($\kappa\partial\tilde{T}/\partial r = \bar{T}u_r$).

These numerical results illustrate graphically the behavior predicted by the Cartesian model. For example, the streamlines plotted all correspond to the same contours of the streamfunction, or in other words the same mass flux. It is therefore obvious that the flows driven through latitudinal forcing are negligible compared with the three other cases. The flows driven by azimuthal forcing appear to be quite strong, although this is merely related to the fact that the linear velocity U_0 corresponding to the imposed (solar) differential rotation is more than two orders of magnitude larger than V_0 at the same latitudes. The flows driven by radial forcing are quite strong, in particular given that the driving velocity W_0 is at least one order of magnitude lower than V_0 at the same latitude. One can also readily see that the flow velocities predicted using type 2 thermal boundary conditions are much stronger than in the case of type 1 thermal boundary conditions. The right-side quadrants reveal the effect of these meridional flows on angular momentum transport in the interior and show the angular velocity profile corresponding to the ultimate steady-state achieved in the radiative interior should the Sun be left to evolve for many flow turnover times under the same applied boundary conditions. Since the turnover time can be considerably longer than the age of the Sun in most cases, these steady states would never in practise be achieved. However, they do reveal two points of particular interest. Firstly, they illustrate how sensitive the interior rotation rate is to the assumed or calculated flow structure, and therefore also to the assumed convective-radiative interfacial boundary conditions. Secondly, they reveal the possibility of unphysical counter-rotation permitted by the linearization of the problem (see §3.6 for a discussion of this effect). This should be taken as a cautionary warning for any linear study of flows and thermal perturbations in the solar radiative interior to always perform a self-consistency check of the validity of the linearization.

5. DISCUSSION AND CONCLUSION

We have studied the penetration of global-scale meridional flows generated in the solar convection zone into the radiative

zone below.

We have attacked the problem via a Cartesian model, as others have done before us, and then verified our results with more complete numerical modeling in the correct geometry. We have extended previous work done by GM04 and McIntyre (2007) by taking into account the full structure of the governing equations and by examining the effect of boundary conditions on the solutions, or in other words, allowing a greater range of convective flows to act as sources for the flows in the radiative interior.

Within a linear formalism, we confirm that the flow pattern in the radiative interior is a linear combination of two types of solutions: (a) a solution that decays away from the convective-radiative interface on a short length-scale related to the Ekman depth, and (b) a solution that decays away from the interface on a much longer length-scale associated with the stratification of the radiative interior. Our more complete treatment of the problem provides accurate expressions for the slowly varying solution. In addition, we find that the *amplitudes* of the rapidly and slowly varying solutions depend sensitively on the choice of dynamical and thermal interfacial forcing.

Forcing by azimuthal and latitudinal shear at the upper boundary lead to both rapidly varying and slowly varying solutions, but with amplitudes that are negligible outside a few Ekman lengths. Forcing by direct radial pumping however can generate flows which are significant outside the Ekman boundary layer and indeed are sufficiently slowly-varying that they may maintain significant flow amplitudes across the whole depth of the radiative zone. The selected thermal boundary conditions at the convective-radiative interface are also found to have significant impact on the interior solution.

In this linear problem, full solutions can be built from combinations of the individual solutions obtained for each different type of boundary forcing that we studied. Thus in principle we should be able to determine the complete flow structure within the radiative interior. However, the problem lies in the selection of the interfacial conditions. We know from helioseismology the amplitude of the average azimuthal flows existing near the base of the convection zone, but know very little of the nature of the meridional flows or of the thermal conditions at that interface. Thus, without a complete model of the whole solar interior which includes the turbulent solar convection zone we can only speculate upon the thermal and dynamical nature of the convective-radiative interface. Instead, when studying a broad range of *plausible* boundary conditions we find that significant penetration depths can be realized.

Previous work by GM04 focused on the effects of a latitudinal source flow only. Our result is in accordance with theirs for this particular type of boundary condition, namely that the flows within the radiative interior are limited to an Ekman depth. However, GM04 conclude that penetration is *always* quenched. Given our analytical and numerical results in the case of other applied boundary conditions, we feel that this conclusion is too strong. Other plausible models of the interface lead to different results concerning the flow amplitudes within the interior. Without better knowledge of the conditions at the convective-radiative interface, it is hard to predict precisely what does happen.

While realistic three-dimensional global models of the solar interior combining radiative and convective regions are not yet numerically achievable, turbulent closure models have been applied to model both azimuthal and meridional flows in most of the solar interior (Kitchatinov & Ruediger, 2005; Rempel,

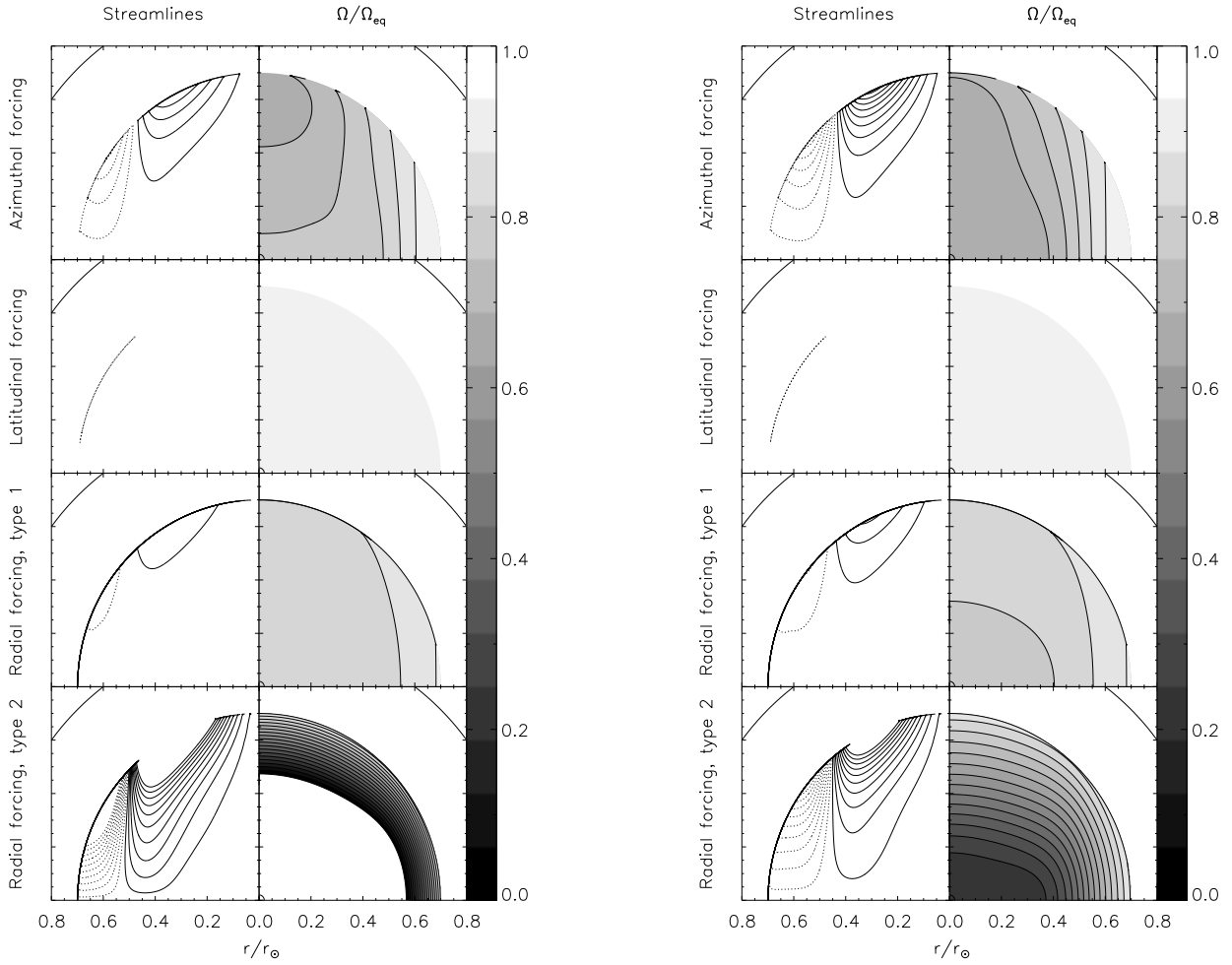


FIG. 5.— Global structure of the flow solutions in the radiative interior of the Sun subjected to a series of different boundary conditions at the convective-radiative interface (at $r = 0.7r_{\odot}$), for fixed value of $f = 10^8$. The left-hand-side set of plots shows solutions for a solar value of the Prandtl number, while the right-hand-side set of plots shows solutions for the case where the thermal conductivity is artificially increased by a factor of four. In each sets of plots, the streamlines are shown in the left-quadrant; the solid lines show clockwise flows, while the dotted lines show counter-clockwise flows. The relative angular velocity normalized by the equatorial value at the convective-radiative interface is shown in the right-quadrant. The “white” region in the final set of boundary conditions actually corresponds to an unphysical counter-rotation. This is an artefact of the linearization of the problem, combined with the high flow velocities in the interior, which would not occur should the fully nonlinear equations be considered.

2005). Using such a model, Ruediger, Kitchatinov & Arlt (2005) studied the penetration of meridional flows into the tachocline. By defining the penetration depth D_{pen} as *the distance from the base of the convection zone to the location of the first reversal in $u_{\theta}(r)$* , they find that $D_{\text{pen}} \sim \sqrt{E_{\nu}}$ and conclude by agreeing with GM04 that the depth of penetration of the flows in the interior is indeed limited to the Ekman solution. However, it is clear from our analysis that D_{pen} as defined by Ruediger, Kitchatinov & Arlt only measures the variation of the rapidly decaying solution (which indeed must vary on an Ekman length). For example, inspection of Figure 1 shows that at a first glance, all of the solutions appear to behave as Ekman solutions, while it is only by looking more closely at the flows deep in the interior (in Figure 3) that one can identify the presence of the slowly decaying solution with a relatively low but nonetheless significant amplitude. We suggest that the predictions of the closure models for flow velocities in the interior could be revisited in the light of our analysis.

Finally, the governing equations in this work have been simplified using two major approximations, which must now be briefly addressed. Firstly, this study assumes the flows to be

in a quasi-steady state. As it was shown by McIntyre (2007) this assumption filters out any transient flows, which could in some circumstances be of much larger amplitude than these steady-state flows (see Spiegel & Zahn, 1992 for example). Therefore our conclusions are likely to underestimate the actual turnover time of transient meridional flows.

Secondly, the momentum and thermal energy equation have been linearized with the consequences described in §2.7, an example of which (the unphysical counter-rotation) is shown in Figure 5. We do emphasize that in the real Sun nonlinear effects would play a role in limiting the amplitude of the meridional and azimuthal flows penetrating into the radiative zone. Therefore our results are consistent with the standard theory that no flows with turnover times faster than the thermal diffusion time are allowed into the radiative zone. This limits the flow turnover time in the tachocline region to a few times 10^5 years, and into the deep interior to a few times 10^7 years.

Neither of these caveats, however, change the main conclusion of our analysis, which is that the penetration of meridional flows into the radiative interior is not necessarily limited to a shallow Ekman depth.

REFERENCES

- Barcilon, V. & Pedlosky, J., 1967, *J. Fluid. Mech.*, 29, 609
 Brown, T. M., Christensen-Dalsgaard, J., Dziembowski, W. A., Goode, P., Gough, D. O. & Morrow, C. A., 1989, *ApJ*, 343, 526
 Brun, A. S., Turck-Chièze, S. & Zahn, J.-P., 1999, *ApJ*, 525, 1032
 Charbonneau, P., 2005, *Living Reviews in Solar Physics*.
 Christensen-Dalsgaard, J., Gough, D. O. & Thompson, M. J., 1991, *ApJ*, 378, 413
 Elliott, J. R. & Gough, D. O., 1999, *ApJ*, 516, 475
 Garaud, P., 2001, PhD Thesis
 available from <http://www.ams.ucsc.edu/~pgaraud/>
 Garaud, P., 2002, *MNRAS*, 335, 707
 Garaud, P. & Rogers, T., 2007, in proceedings of the meeting “Unsolved Problems in Stellar Astrophysics”, held in Cambridge, July 2007.
 Giles, P. M., Duvall, T. L., Jr., Scherrer, P. H. & Bogart, R. S., 1997, *Nature*, 390, 52
 Gilman, P. A., Morrow, C. A., & DeLuca, E. E., 1989, *ApJ*, 338, 528
 Gilman, P. A. & Miesch, M. S., 2004, *ApJ*, 611, 568
 Gough, D. O. & McIntyre, M. E., 1998, *Nature*, 394, 755
 Hughes, D. W., Rosner, R. & Weiss, N. O., 2007, *The Solar Tachocline*, CUP.
 McIntyre, M. E., 2007, in *The Solar Tachocline*, pp. 183-212, eds. Hughes, D. W., Rosner, R. & Weiss, CUP.
 Miesch, M. S., Elliott, J. R., Toomre, J., Clune, T. L., Glatzmaier, G. A. & Gilman, P. A., 2000, *ApJ*, 532, 593
 Rempel, M., 2005, *ApJ*, 622, 1320
 Spiegel, E. A. & Zahn, J.-P., 1992, *A&A*, 265, 106